COMSOL CONFERENCE 2023 MUNICH

Modeling and simulation study of a fixed-bed catalytic reactor for the hydrogenation of CO_2 to CH_4

I. Lacarra-Etxarri, E. Gómez-Bravo, J. A. González-Marcos, J. R. González-Velasco, B. Pereda-Ayo
Department of Chemical Engineering, University of the Basque Country, Leioa, Bizkaia, Spain.

Abstract
Power-to-Gas technology intends to store the surplus electric energy from renewable sources. This energy is used to obtain H_2 through water electrolysis, which will later be reacted with captured CO_2 to obtain Synthetic Natural Gas (SNG). The CO_2 hydrogenation or methanation reaction involved in this technology is a highly exothermic and reversible reaction. Thus, efficient heat management of the reactor is necessary to avoid hot spots and maximize CH_4 production at the reactor outlet. The use of simulation software can be a very useful tool to assist the design of efficient reactors. In this work, several models to simulate the CO_2 hydrogenation reaction have been developed with the commercial software COMSOL Multiphysics®. Using the Chemical Reaction Engineering Module and its associated interfaces, the CO_2 hydrogenation reaction has been simulated in a fixed-bed reactor with a 10% Ni/alumina catalyst. First, a zero-dimensional model was used to simulate isothermal, adiabatic and non-isothermal plug-flow reactors. Then, one-dimensional (1D) models were implemented to simulate gas-phase reaction in the absence or presence of a porous medium, which consider mass and energy transport in the axial direction of the reactor. Specifically, it was observed that energy transport in the axial direction significantly changes the conversion and temperature profiles. Finally, two-dimensional (2D) gas-phase models were implemented, considering mass and energy transport in both radial and axial directions of the reactor.
Keywords: Simulation, CO_2 hydrogenation, Fixed-bed reactor.

Introduction
The world is undergoing an unprecedented energy revolution driven by social, environmental, and economic factors [1]. The increasing energy demand is primarily met by oil, gas, and coal. However, the consequences of climate change resulting from high CO_2 emissions are becoming increasingly evident.
Therefore, renewable energy sources are gaining importance. However, the challenge remains in the gap between supply and demand [2]. During periods of low wind and low or no solar radiation, electricity production does not meet the demand, while high-wind and sunny periods can result in surplus electricity. Therefore, solutions for storage of renewable energy are of great interest to balance fluctuating production and energy use [3].
One option for storing excess electricity is its conversion into chemical energy through "Power to Gas" (PtG) technology [4]. In the first step, renewable energy sources can be used to generate H_2 through water electrolysis. However, H_2 requires special materials for storage, and its volumetric energy density is low [5]. Hence, the later conversion of H_2 with CO_2 into methane (synthetic natural gas, SNG) comes into play: captured CO_2 can be combined with H_2 and catalytically converted into SNG. The methanation reaction or Sabatier reaction is shown in Equation (1).

$$CO_2+4H_2 \leftrightarrows CH_4+2H_2O \quad (1)$$

The ability to use existing natural gas infrastructure for storing and transporting SNG to end users provides a critical advantage over other concepts. Figure 1 shows a diagram of the PtG technology.
Considering this potential application, this work studies the direct hydrogenation of CO_2. It should be noted that the hydrogenation of CO_2 is a strongly exothermic reversible reaction with a reduction in the number of moles, making it thermodynamically favored at low temperatures and high pressures. Kinetics are also favored at high pressures, but low temperatures reduce the rate. Therefore, heat management is crucial to prevent catalyst damage and effectively use the released heat.

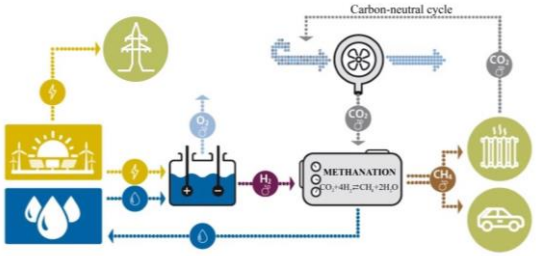

Figure 1. Diagram of the "Power to Gas" process.

Since CO_2 methanation is the central step in PtG, extensive research has focused on reactor design and optimization [6]. In methanation processes, multitube (fixed-bed) reactors appear as the standard concept due to their simple design and direct manufacturing. Because of the high exothermicity of the Sabatier reaction, the shell-and-tube configuration appears as a practical and effective engineering solution for temperature control [7]. Conventional design method for multitube fixed-bed reactors assumes that a single tube can be considered an adequate representation of the entire system.
Given all the above, simulation is a valuable tool for reactor design and the selection of optimal operating conditions without the need for physical materials.

This work has focused on the application of the commercial simulation software COMSOL Multiphysics®, to create models that replicate a fixed-bed methanation reactor.

Methodology

Before the construction of the models, some general specifications have been made, which will be implemented in all models. A thermodynamic system has been developed specifying the compounds in the reactive mixture (CH_4, CO_2, H_2 and H_2O), a material containing the gas phase properties and the chemistry modules are set from this thermodynamic system.

For each component of the simulation, the conversion and the gas velocity have been specified as variables using Equations (2) and (3).

$$X_{CO_2} = \frac{w_{0,CO_2} - w_{CO_2}}{w_{0,CO_2}} \quad (2)$$

$$u = \frac{Q_0 \rho_0}{A_c \rho} \quad (3)$$

Zero-dimensional model

The simplest models are created in zero-dimensional components. The reaction engineering module allows to create plug-flow reactor models within this zero-dimensional framework. In this work, three reactor models were created: an isothermal reactor, an adiabatic reactor and a reactor with heat exchange with the outside furnace. Equation (4) defines the mass balance, while Equations (5) and (6) define the energy balance.

$$\frac{dF_i}{dV} = R_i \quad (4)$$

$$C_p \sum_i F_i \frac{dT}{dV} = Q + Q_{ext} \quad (5)$$

$$Q = -\sum_j H_j r_j \quad (6)$$

The boundary conditions in the zero-dimensional model are equal to the feed conditions for mass fraction and temperature.

A constant temperature was set for the isothermal model, while for the adiabatic one heat exchange (Q_{ext}) was set to 0 and for the model considering heat exchange Q_{ext} was calculated with Equation (7).

$$Q_{ext} = -U\left(T - T_{ext}\right) \quad (7)$$

where U is the global heat exchange coefficient and T_{ext} is the furnace temperature.

The Sabatier reaction (Equation (1)) was specified in the reaction node. The reaction kinetics follow Equation (8).

$$r_{CO_2} = k^f \cdot \left([CO_2]^n [H_2]^{4n} - \frac{[CH_4]^n [H_2O]^{2n}}{\left[K_{eq0j}(T)\right]^n} \right) \quad (8)$$

Since the reaction order (n) is 0.702 and the module demands an integer, the concentration values have been adimensionalized and the order has been set to 0. The kinetic constant is calculated with the Arrhenius equation and the equilibrium constant is calculated by COMSOL. A parametric sweep is performed to find the best temperatures in the reactor inlet for each of those models.

One-dimensional model

Adding the reactor length dimension allows to increase the complexity of the model notoriously. In those models various modules work together to simulate the reactor. In the chemistry module, the characteristics of the chemical reaction are introduced, along with some properties of the species; similar to the reaction engineering module described before. The transport of concentrated species interface calculates the mass fractions of all the species of the reactive mixture when none of those can be considered as a solvent. This module considers the diffusion of the species; this module uses Equations (9) and (10) to calculate the species concentration.

$$\nabla \cdot j_i + \rho\left(u \cdot \nabla\right) w_i = R_i \quad (9)$$

$$j_i = -\left(\rho D_i^m \nabla w_i + \rho w_i D_i^m \frac{\nabla M_n}{M_n} - j_{c,i} \right) \quad (10)$$

To calculate the temperature in each point of the axial direction, the heat transfer module is used. In Equation (11), the energy balance is expressed, through which the temperature is calculated. The conductive heat flux used in the balance is calculated through Equation (12). In the Heat Source Node, the heat generated and dissipated throughout the reactor is calculated with Equation (13).

$$A_c \rho C_p u \cdot \nabla T + \nabla \cdot q = A_c Q + q_0 \quad (11)$$

$$q = -A_c k_f \nabla T \quad (12)$$

$$q_0 = A_i \cdot \left[Q - U \cdot \left(T - T_{ext} \right) \right] \quad (13)$$

Due to the specific configuration of the reactor under investigation and the presence of axial transport processes, it becomes necessary to employ mass and energy fluxes as inlet boundary conditions, rather than specifying values for mass fraction and temperatures. To solve the system, the boundary conditions proposed by Danckwerst are applied. At the reactor entrance it is considered that there is no reaction as shown in Equation (14) and (15). At the reactor outlet it is stablished a non-flux condition.

$$w_{bnd,i} : - \int_{\partial\Omega} n \cdot \left(j_i + \rho u w_{bnd,i} \right) dA_c = J_{in,i} \quad (14)$$

$$-n \cdot q = \rho \Delta H u \cdot n \quad (15)$$

For both modules, species transport and heat transfer, a porous media variation is also used. With this feature, the mass diffusion and thermal conductivity coefficients are corrected to take the porous media into account, using Equations (16) to (18).

$$D_{e,ik} = \frac{\varepsilon_p}{\tau_f} D_{ik} \quad (16)$$

$$\tau_f = \varepsilon_p^{-1/3} \quad (17)$$

$$k_{eff} = \varepsilon_p k_f + \theta_s k_s \quad (18)$$

Finally, an interface to calculate fluid flow has been implemented. In this case, the Darcy's Law module is used, which calculates pressure and flow velocity in a porous medium through Equations (19) to (21).

$$\nabla \cdot \rho u = Q_m \tag{19}$$

$$u = -\frac{\kappa}{\mu}\nabla p \tag{20}$$

$$\kappa = \frac{d_p^2}{180}\frac{\varepsilon_p^3}{1-\varepsilon_p^2} \tag{21}$$

Axisymmetric two-dimensional model

Considering one tube in a multitube reactor a cylinder can describe the geometry of the model. A rectangle is drawn in the geometry node, a cylinder is the outcome of its rotation.

The same modules as before have been used to define the chemistry, the species transport in porous media and heat transfer in porous media.

The brinkman equations module is used to calculate the fluid flow in porous media through Equations (22) and (23).

$$0 = -\nabla p + \nabla\cdot\left[\frac{1}{\varepsilon_p}\left\{\mu\left(\nabla u + (\nabla u)^T\right) - \frac{2}{3}\mu(\nabla\cdot u)I\right\}\right] - \left(\mu\kappa^{-1} + \frac{Q_m}{\varepsilon_p^2}\right)u + F \tag{22}$$

$$\nabla\cdot(\rho u) = Q_m \tag{23}$$

Simulation conditions

Simulation conditions have been set to replicate a lab-scale reactor. The reactor is placed in a furnace and its inner diameter is 9 mm and the fixed catalytic bed presents a length of 25 mm. The reactor is loaded with 10% nickel on alumina catalysts. The porosity of the bed is 0.47 and its density 0.65 g/cm^3, therefore the mass of catalyst is 1,03 g. The feed stream is composed of hydrogen and carbon dioxide in stoichiometric proportions, that is, four moles of H_2 enter for every mole of CO_2. The CO_2 flow rate is 100 mL/min at 298 K. The value of the global heat transfer coefficient between the reactor and the furnace U is 10 W/(m^2·K) for all the simulations.

Results and Discussion

Zero-dimensional model

As a first approach, zero-dimensional models will be used to simulate isothermal, adiabatic and non-isothermal (with heat exchange) plug-flow reactors. These models will be used to analyze the progress of the reaction and identify the challenges of the reactor to maximize CO_2 conversion.

Figure 2 shows the CO_2 conversion profiles along the reactor length and Figure 3 shows the temperature profiles. The inlet temperature of each reactor (isothermal, adiabatic or heat exchange) corresponds to the temperature that maximizes CO_2 conversion at the reactor outlet.

As observed in Figure 2, the evolution of CO_2 conversion with reactor length varies significantly depending on the reactor type. In the isothermal reactor, the conversion rapidly increases at the reactor inlet in a strict kinetic control regime. The fact that the reactor is isothermal (all the heat generated is supposed to be removed) avoids thermodynamic restrictions and CO_2 conversion asymptotically approaches equilibrium at the reactor outlet. At the optimum reaction temperature of 453°C, the CO_2 conversion reaches 0.75 at the reactor outlet.

In the adiabatic reactor, with a lower inlet temperature (248 ºC) with respect to the isothermal reactor (453 ºC), conversion grows slowly limited by kinetics. As the reaction advances, temperature rises due to the release of heat of reaction, which accumulates in the gas phase and promotes kinetics. Therefore, there is an exponential growth of conversion and temperature. The growth suddenly stops when reaction reaches the thermodynamic equilibrium at high temperatures. Beyond this point, conversion and temperature remain constant until the outlet due to the adiabatic nature of the reactor. The maximum CO_2 conversion at the outlet of the adiabatic reactor is 0.37, significantly lower than the isothermal reactor (0.75), which evidences the need for an efficient heat management of the reactor.

In the reactor with heat exchange, the inlet temperature that maximizes CO_2 conversion is 279 ºC. Due to the higher inlet temperature with respect to the adiabatic reactor (248 ºC), CO_2 and temperature profiles are advanced to earlier positions of the reactor length and a hot spot is observed

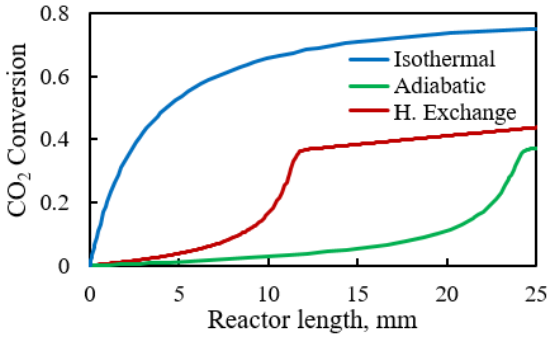

Figure 2. CO_2 conversion profile along the reactor length for isothermal, adiabatic and heat exchange reactors.

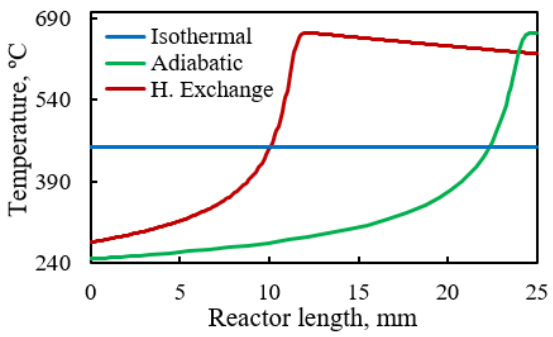

Figure 3. Temperature profile along the reactor length for isothermal, adiabatic and heat exchange reactors.

around 12 mm in Figure 3. Due to the ability of the reactor to remove heat, reaction can further progress as heat is removed, reaching an outlet conversion of 0.44, higher than that observed for the adiabatic reactor. The heat exchange reactor, as a more realistic approach to simulate industrial reactors, will be more deeply analyzed in the following sections, developing models that are more accurate for describing the physicochemical features occurring in the reactor.

One-dimensional model

1D models can consider mass and energy transport along the axial reactor coordinate. To verify the consistency of the 1D model and its correct implementation, the obtained results were compared with the 0D model from the previous section. First, the individual effect of mass and energy transport was analyzed. CO_2 conversion and temperature profiles for the 1D model with mass transport (1D-k=0; $D_{Maxwell}$) can be observed in Figures 4 and 5. The individual diffusion coefficient for each species (CO_2, H_2, CH_4 and H_2O) was estimated using the Maxwel-Stefan model. The consideration of mass transport smooths the CO_2 conversion profile due to the back mixing effect (light blue line). Mass transport also influences the temperature profile due to the more gradual release of reaction heat into the gas phase. Consequently, the hot spot is slightly shifted towards latter positions of the reactor.

The consideration of energy transport (1D-k_{chem}; D=0), with an estimated thermal conductivity of the fluid around 0.3 W/m·K, modifies drastically the CO_2 conversion and temperature profiles (green line). Due to the heat transport phenomena, heat is distributed along the reactor length and the hot spot is advanced to a reactor length of 1.8 mm. The fact that the hot spot is moved to earlier positions, leaves behind a longer fraction of the reactor to refrigerate the reaction mixture, which displaces the equilibrium and permits the reaction to further progress, achieving an outlet conversion of 0.48. Note that, although gases are fed at 279 ºC, the reactor inlet temperature is as high as 557 ºC, which evidences the importance of heat transport. At this point, it is worth mentioning that boundary conditions defined by Danckwerst are necessary to be applied, and providing a good initial guess of the solution is of vital importance to succeed in the resolution.

Finally, the joint consideration of mass and energy transport (1D-k_{chem}; $D_{Maxwell}$) is also included in Figure 4 and 5 by a red line. As already discussed, the inclusion of mass transport slightly retards the hot spot and the back mixing effect is now (with the inclusion of energy transport) more evident. Note that the CO_2 conversion at the reactor inlet is 0.12. The presence of products at the reactor entrance slows down the reaction rate, and consequently, the reactor inlet temperature is somewhat lower (522 ºC) with respect to the model that only accounts for energy transport.

Figure 6 shows the evolution of CO_2, H_2, CH_4 and H_2O molar fractions with the reactor length. Note that the molar fraction of products (CH_4 and H_2O) is already higher than zero at the reactor entrance, which evidences the back mixing effect. Besides, as the Maxwell-Stefan model individually estimates the diffusion rate of each species, the stoichiometric relation of CO_2 and H_2 found in the feed stream can be modified along the reactor. In fact, it can be observed that the H_2 molar fraction deviates from the $4H_2$:CO_2 of the feed stream. A lower H_2 molar fraction is observed at the reactor entrance due to its higher diffusion coefficient, which tends to homogenize its molar fraction along the reactor length. The independent consideration of diffusion rates for each species leads to changes in both kinetics and thermodynamics, culminating in a hot-spot temperature of 669 ºC (Figure 5) and an outlet CO_2 conversion of 0.47 (Figure 4).

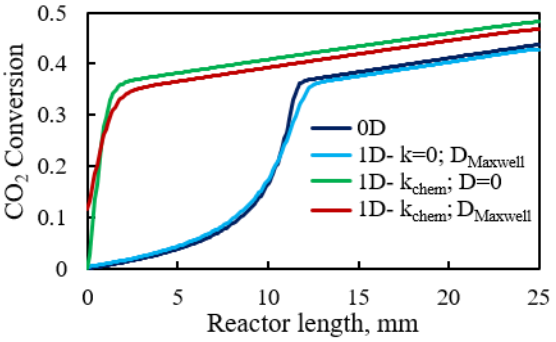

Figure 4. CO_2 conversion profile along the reactor length for 1D models considering mas and energy transport.

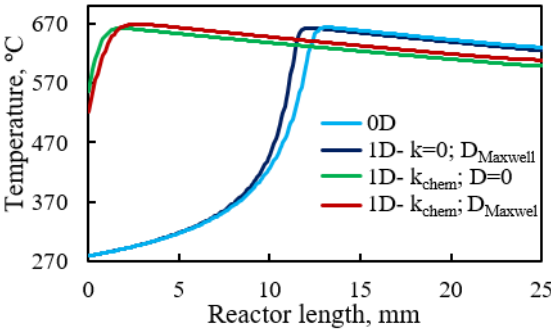

Figure 5. Temperature profile along the reactor length for 1D models considering mas and energy transport.

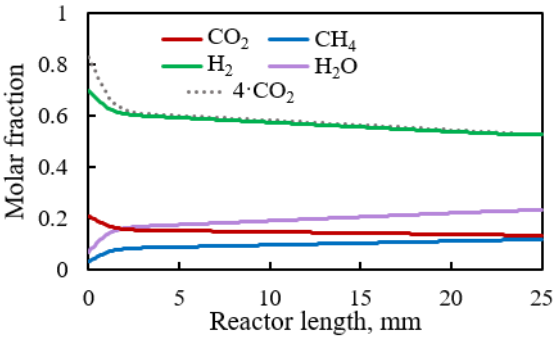

Figure 6. Evolution of reaction species molar fraction along the reactor length using Maxwell-Stefan diffusion model.

Until now, the developed models have not considered the presence of a catalyst in the reactor. However, CO2 hydrogenation is always catalyzed by a solid to enhance the reaction rate. Besides, the presence of a solid catalyst can modify mass and energy transport phenomena. Thus, the following 1D model considers the presence of a porous medium along with mass and energy transport in the axial direction.

As can be observed in Figure 7 and 8, the presence of a porous medium (1D-k_{porous}; $D_{Maxwell-porous}$) modifies CO_2 conversion and temperature profiles with respect to those obtained in the absence of a porous medium (1D-k_{chem}; $D_{Maxwell}$). Note that the presence of a porous material can particularly modify energy transport, because the solid phase considerably enhances the conductivity of the medium. In fact, the conductivity is estimated to be around 3.1 W/m·K, significantly higher than that observed for the fluid phase (0.3 W/m·K). Therefore, the heat generated can be easier conducted throughout the reactor length and the observed temperature at the reactor inlet is increased up to 644 ºC, considerably higher than that observed in the absence of a porous medium (522 ºC). Besides, the temperature at the rear of the reactor is lower for the porous medium model, again facilitated by heat conduction, which avoids thermodynamic limitations and promotes CO_2 conversion at earlier positions of the reactor. Overall, the porous medium enhances heat conduction and allows the reactor to approach an isothermal operation. In fact, the hot spot temperature drops to 655 ºC, and the maximum temperature gradient across the whole reactor length is lowered below 46 ºC.

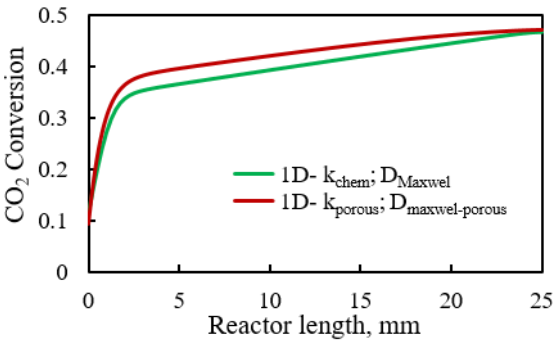

Figure 7. CO_2 conversion profile along the reactor length for 1D models in the presence or absence of a porous medium.

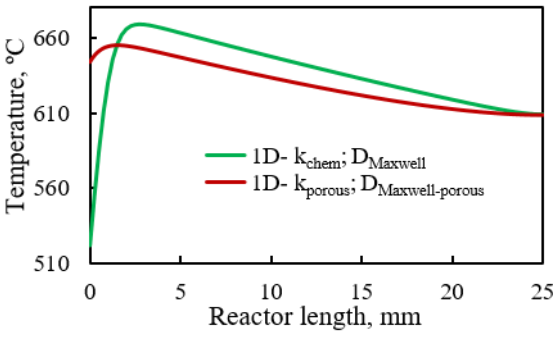

Figure 8. Temperature profile along the reactor length for 1D models in the presence or absence of a porous medium.

Axisymmetric two-dimensional model

The one-dimensional models developed in the previous section neglect CO_2 conversion and temperature gradients in the radial axis of the reactor. However, radial mass and heat transport can also play a critical role in the performance of the reactor. Specifically, as heat exchange occurs between the reactor wall and the surroundings, radial temperature gradients have to be cautiously analyzed.

The following axisymmetric two-dimensional model considers mass and energy transport in both radial and axial directions of the reactor. Figure 9 shows the velocity profile in the reactor axial and radial coordinates, whereas Figures 10 and 11 show conversion and temperature profiles.

As can be observed in Figure 9, velocity gradients are absent in the radial direction of the reactor. The gas-flow velocity only changes in the axial direction, primarily due to temperature effects but also due to conversion effects, taking into account the reduction of the total number of moles with the extension of the reaction. The maximum velocity is observed near the reactor entrance, in line with the hot spot temperature observed in Figure 11. Afterwards, the gas-flow velocity decreases as the reaction mixture is cooled down. The absence of radial gas-flow velocity is a consequence of the slip condition imposed at the reactor wall, which neglects viscous effects. If the non-slip condition is imposed, only a very thin and abrupt velocity profile is observed near the reactor wall but does not influence the conversion and temperature profiles.

On the contrary, Figures 10 and 11 show the presence of radial CO_2 conversion and temperature profiles, with the exception of the reactor entrance (L=0), where CO_2 conversion is 0.08 irrespective of the radial position. This is not the case of

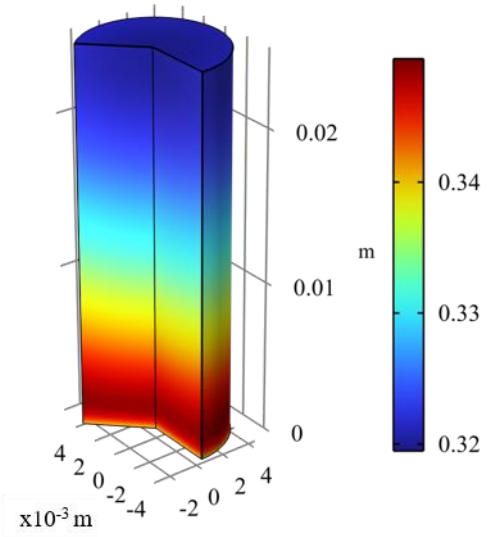

Figure 9. Radial and longitudinal velocity profiles for 2D model.

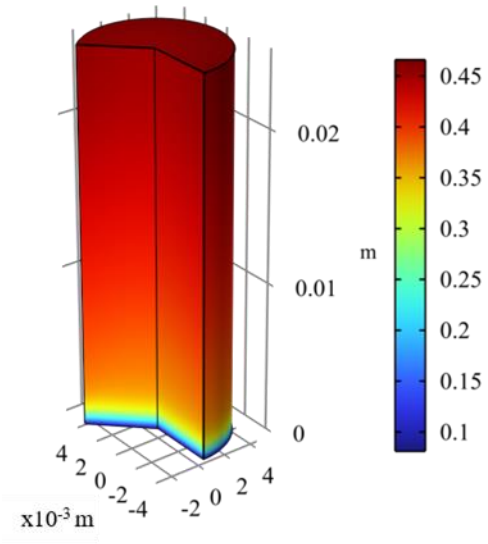

Figure 10. Radial and longitudinal conversion profiles for 2D model.

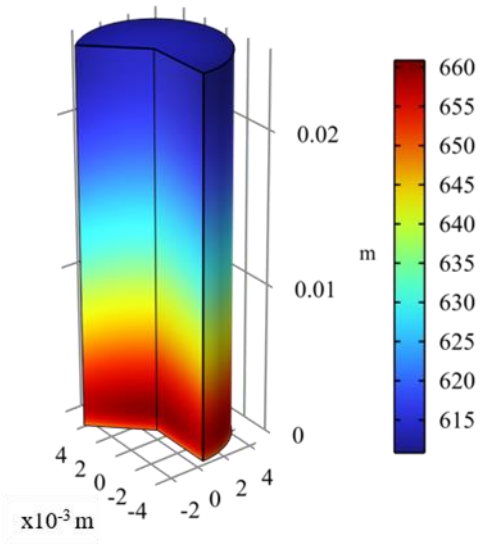

Figure 11. Radial and longitudinal temperature profiles for 2D model.

temperature, which shows a radial profile even at the reactor entrance. At the reactor longitudinal axis (r=0) temperature is 650 ºC, whereas at the reactor wall (r=R) temperature is 649 ºC. Note that CO_2 conversion is higher than zero and temperature is higher than the feed stream temperature (279 ºC) due to mass and energy transport effect in the axial direction. As already observed in previous sections, Figure 11 shows a hot spot near the reactor entrance (L=1.4 mm), where radial conversion and temperature gradients are observable. As refrigeration occurs through the reactor walls, the gas mixture is cooler at the reactor wall (658 ºC) with respect to the axial coordinate (661 ºC), as already observed at the reactor entrance. The observed temperature gradient induces radial CO_2 conversion gradients. A lower temperature at the wall (r=R) allows a higher CO_2 conversion equilibrium, achieving a CO_2 conversion of 0.34. On the contrary, thermodynamic restrictions are higher at the reactor axial coordinate (r=0), where conversion results in 0.33. After the hot spot, radial CO_2 conversion and temperature profiles are maintained throughout the whole reactor length. The average conversion and temperature at the reactor outlet are 0.46 and 612 ºC.

Conclusions

From the completion of this work, a series of conclusions have been drawn, which are presented below.

Zero-dimensional isothermal, adiabatic and heat exchange plug-flow reactors have been modeled to analyze the progress of the reaction and identify the challenges of the reactor to maximize CO_2 conversion. Due to the highly exothermic nature of the CO_2 hydrogenation to CH_4, a hot spot is evident in the heat exchange reactor model. The temperature increases favors kinetics but has a negative effect on thermodynamics, evidencing the critical role of heat management to maximize CH_4 production.

A one-dimensional reactor model has been constructed and simulated. Firstly, the effect of considering mass and heat transport in the longitudinal axis of the reactor has been analyzed, comparing the results with ideal zero-dimensional models. The consideration of heat transfer induces drastic changes of CO_2 conversion and temperature profiles along the reactor length. In fact, the longitudinal position of the hot spot observed for the zero-dimensional model is shifted towards the reactor entrance. Temperatures as high as 522 ºC are observed at the reactor entrance when the gas feed stream is fed at 279 ºC. Although to a minor extent, mass transport also modifies CO_2 conversion and temperature profiles. Due to the back mixing effect, CO_2 conversion and temperature profiles tend to be smoother. The consideration of the presence of a porous medium in the reactor enhances specifically heat transport, due to the higher conduction coefficient of the solid. As a result, the hot spot is further shifted towards the reactor entrance, and the temperature is 644 ºC at the reactor entrance.

Finally, an axisymmetric two-dimensional model has been constructed and simulated, considering mass and energy transport in both radial and axial directions of the reactor. Velocity gradients are absent in the radial direction of the reactor. The gas-flow velocity only changes in the axial direction, primarily due to temperature effects. On the contrary, CO_2 conversion and temperature gradients are observable in the radial direction. As refrigeration occurs through the reactor walls, the gas mixture is cooler at the reactor wall (r=R) with respect to the axial coordinate (r=0). This also affects thermodynamics, imposing higher restrictions for the regions with more elevated temperatures. Consequently, CO_2 conversion is promoted near the reactor wall and tends to decrease as approaches the axial coordinate of the reactor.

COMSOL Multiphysics has proven to be an effective simulation tool with a user-friendly

interface that allows for the implementation of increasingly complex models. The software's database, both for materials and thermodynamics, has been very helpful and reliable. In the near future reactor models that account for the presence of the catalysts will be implemented. Those heterogeneous models will be valuable to analyze mass and heat transfer resistances among the fluid and the solid phase. Additionally, temporal studies should be conducted to understand the reactor's response to variations in the hydrogen flow rate, which depends on the surplus of renewable energy.

Nomenclature

$[i]$	Concentration of species i, mol/m^3
C_p	Molar heat capacity of the gas mixture, J/(mol·K)
D_i^m	Diffusion coefficient of each species in the mixture, m^2/s
$D_{e,ik}$	Effective Maxwell-Stefan diffusivity of species i and k, m^2/s
D_{ik}	Maxwell-Stefan diffusivity of species i and k, m^2/s
d_p	Particle diameter, m
F	Influence of gravity and other volume forces, kg/(m^2·s^2)
F_i	Molar flux of the compounds, mol/s
H_j	Reaction enthalpy, J/mol
$J_{in,i}$	Inlet diffusive flux, kg/(m^2·K)
j_i	Relative mass flux, kg/(m^2·K)
$j_{c,i}$	Diffusive mass flux correction, kg/(m^2·K)
K_{eq0j}	Equilibrium constant
k_{eff}	Effective thermal conductivity, W/(m·K)
k_f	Thermal conductivity of the fluid, W/(m·K)
k^f	Kinetic constant, mol/(s·m^3)·(m^3/mol)^{5n}
k_s	Thermal conductivity of the solid, W/(m·K)
M_n	Mean molar mass, kg/mol
n	Reaction order
p	Pressure, Pa
Q_0	Volumetric flow at the inlet, m^3/s
Q	Reaction heat, J/s
Q_{ext}	External heat, J/s
Q_m	Volumetric mass source, kg/(m^3·s)
q_0	Heat flow to the interior, W/m
R_i	Species generation rate, mol/(m^3·s)
r_j	Reaction rate, mol/(m^3·s)
A_c	Reactor cross section, m^2
T	Temperature, K
T_{ext}	Furnace temperature, K
U	Global heat transfer coefficient, W/(m^3·K)
u	Gas velocity, m/s
V	Reactor volume, m^3
w_i	Mass fraction of species i
$w_{bnd,i}$	Mass fraction of species i in the inlet
$w_{0,i}$	Feed mass fraction of species i
X_{CO_2}	CO_2 conversion
ε_p	Bed porosity
θ_s	Volumetric fraction of the solid
κ	Permeability, m^2
μ	Dynamic viscosity, Pa·s
ρ	Gas density, kg/m^3
ρ_0	Gas density at the inlet, kg/m^3
τ_f	Tortuosity, dimensionless

References

[1] V. Soto, C. Ulloa and X. Garcia, "A CFD Design Approach for Industrial Size Tubular Reactors for SNG Production from Biogas (CO2 Methanation)," *Energies (Basel)*, vol. 14, *(19)*, pp. 6175, 2021. Available: https://search.proquest.com/docview/2580982599. DOI: 10.3390/en14196175.

[2] G. Tauer, C. Kern and A. Jess, "Transient Effects during Dynamic Operation of a Wall-Cooled Fixed-Bed Reactor for CO2 Methanation," *Chemical Engineering & Technology*, vol. 42, *(11)*, pp. 2401-2409, 2019. Available: https://onlinelibrary.wiley.com/doi/abs/10.1002/ceat.201900367. DOI: 10.1002/ceat.201900367.

[3] S. Schiebahn *et al*, "Power to gas: Technological overview, systems analysis and economic assessment for a case study in Germany," *International Journal of Hydrogen Energy*, vol. 40, *(12)*, pp. 4285-4294, 2015. Available: https://dx.doi.org/10.1016/j.ijhydene.2015.01.123. DOI: 10.1016/j.ijhydene.2015.01.123.

[4] T. Schaaf *et al*, "Methanation of CO2 - storage of renewable energy in a gas distribution system," *Energ Sustain Soc*, vol. 4, *(1)*, pp. 2, 2014. Available: https://link.springer.com/article/10.1186/s13705-014-0029-1. DOI: 10.1186/s13705-014-0029-1.

[5] J. Töpler and J. Lehmann, *Hydrogen and Fuel Cell : Technologies and Market Perspectives.* (1st ed. 2016 ed.) 2016Available: https://library.biblioboard.com/viewer/83264afd-bd43-11ea-88d8-0a28bb48d135. DOI: 10.1007/978-3-662-44972-1.

[6] S. Rönsch *et al*, "Review on methanation – From fundamentals to current projects," *Fuel (Guildford)*, vol. 166, pp. 276-296, 2016. Available: https://dx.doi.org/10.1016/j.fuel.2015.10.111. DOI: 10.1016/j.fuel.2015.10.111.

[7] A. Fache *et al*, "Optimization of fixed-bed methanation reactors: Safe and efficient operation under transient and steady-state conditions," *Chemical Engineering Science*, vol. 192, pp. 1124-1137, 2018. Available: https://dx.doi.org/10.1016/j.ces.2018.08.044. DOI: 10.1016/j.ces.2018.08.044.

Acknowledgements

Support for this study was provided by Project PID2019–105960RB-C21 MCIN/AEI /10.13039/501100011033 and the Basque Government (Project IT1509-2022). One of the authors (EGB) also acknowledges the Spanish Ministry of Universities for her PhD grant (FPU 20/06668).